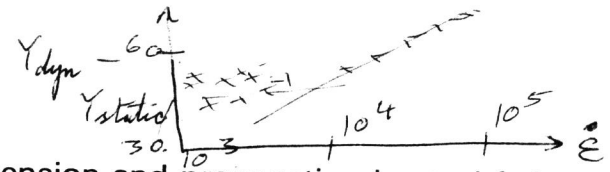

Ductile crack extension and propagation in steel foil

G. T. HAHN, M. F. KANNINEN and A. R. ROSENFIELD
Battelle Memorial Institute, Columbus Laboratories, Columbus, Ohio

Summary

The fracture behavior of cold-rolled steel foil is examined experimentally and in theoretical terms. The experiments reveal the strain distribution ahead of cracks and show that crack extension and stable crack growth proceed with constant crack-tip strain and displacement. The speed of unstable crack propagation appears to depend on the rate dependence of flow and other properties of the material within the plastic zone ahead of the crack. The Dugdale model is extended to include finite plate effects and a Bridgeman necking correction. Both of these factors as well as the rate dependence of yielding are shown to have profound effects on crack speed.

Introduction

Although a full three-dimensional elastic-plastic treatment of a cracked body is not yet in sight, progress has been made in understanding flow and fracture at a crack tip. This has been accomplished with the aid of analyses which are simpler but not as general. The Dugdale model has been particularly useful in this respect. Complications such as strain hardening, the rate sensitivity of flow stress, and finite plate effects have been treated. Furthermore, the predictions of this model have lent themselves to experimental verification.

This paper compares several extended versions of the Dugdale model with experiments on cold-rolled steel foil – a material which is attractive for a number of reasons. Most importantly, cracks in the foil develop narrow wedge-shaped plastic zones which are like those of the Dugdale model. In addition, the steel foil undergoes large plastic strains prior to cracking but necks as soon as it yields. Because the deformation proceeds by flow through-the-thickness, the crack-tip strain distribution can be measured by monitoring the foil thickness locally while the foil is under load. The neck also confines plastic deformation to a relatively small volume, reducing the energy required for ductile cracking and facilitating the study of catastrophic ductile crack propagation in small test coupons.

The paper deals with local yielding prior to cracking, the onset of stable crack extension, stable growth, and rapid propagation. It examines the significance of the crack-tip strain, displacement, and local instability, the relevance of classical fracture mechanics, and the processes limiting the ductile crack speed. The results, although strictly applicable only when through-the-thickness deformation (plane stress) dominates, illuminate basic relations underlying crack extension in all situations.

Analytical techniques

Dugdale modeled [1] plastic relaxation at the ends of a crack by regions which are thin extensions of the crack itself. The key relation results from abolishing the singularities at the ends of the crack. For a crack of length $2c$ in a body subjected to a uniform tensile stress T at infinity the relation can be written

$$\frac{c}{c+l} = \cos\frac{\pi}{2}\frac{T}{Y} \tag{1}$$

where l denotes the length of the plastic zones and Y is the yield stress of the material. A continuation of Dugdale's analysis to obtain the crack opening displacements was presented by Goodier and Field [2]. In particular, they found for the displacement at the crack tip

$$v_c = \frac{4cY}{\pi E}\log\frac{c+l}{c} \tag{2}$$

where E is the elastic modulus.

Stationary cracks

To account for strain-hardening, Rosenfield, *et al.* [3] superposed simple Dugdale solutions to obtain a flow stress which varied in a step-wise manner along the length of the plastic zone. This superposition method is also used here. The displacements under step-wise loading are obtained from Equation 12 of Reference 3 for which Equation 2 represents a special case. Rosenfield, *et al.* required a supplementary model for necking within the plastic zone to relate the displacement to the strain, but in the present study a relation is obtained from actual measurements (Equation 5, Table 1). The load carrying capacity of each point in the plastic zone is connected to the strain and the flow stress at that point by way of Equation 7, Table 1. This relation has incorporated a Bridgeman correction as discussed below. The final links are provided by the actual stress-strain characteristics of the material (Equation 3, Table 1) and a specified critical crack-tip strain.

Propagating cracks

The superposition method is also the basis for a quasi-static analysis of a propagating ductile crack in which dynamic effects are confined to the rate dependence of the flow stress. Since experimentally measured ductile crack speeds in steel foil have not exceeded 400 ft per sec (or 0·05 the Rayleigh velocity), the quasi-static treatment is supported by a solution given by Kanninen [8]. This solution, obtained from the Sneddon-Radok dynamic elasticity equations for a Dugdale crack moving at a constant

speed in the infinite plate, shows that the difference between static and dynamic stress fields is negligible for speeds in this range.

Kanninen, *et al.* [4] compared the quasi-static model with experiments on steel foil and found that the predictions of the analysis were reasonable. Further calculations have now been made and these consider three major

Table 1.
Mechanical properties of cold rolled steel foil

Flow properties [4, 5]

Static yield strength (a): $Y_S = 105$ ksi

Dynamic yield strength (b):

$$\left.\begin{aligned} Y &= Y_S + A + D_1 \log_{10}\dot{\epsilon},\ 1 \geq \dot{\epsilon} \\ Y &= Y_S + A + D_2 \log_{10}\dot{\epsilon},\ 1110 \geq \dot{\epsilon} \geq 1 \\ Y &= Y_S + F\dot{\epsilon},\ \dot{\epsilon} \geq 1110 \\ A &= 6\text{ ksi},\ D_1 = 2\text{ ksi},\ D_2 = 8\text{ ksi} \\ &10\text{ psi-sec} \lesssim F \lesssim 25\text{ psi-sec} \end{aligned}\right\} \tag{3}$$

True flow strength (c): $\sigma = Y_S + \phi\epsilon,\ \phi = 30$ ksi (4)

Plastic zone properties

Strain-displacement relation (d):

$$\epsilon = \log_e\left(\frac{1}{1 - Bv}\right),\ B = 950\text{ in}^{-1} \tag{5}$$

Foil-half-thickness to neck-radius ratio (e): $\frac{a}{R} = 2\epsilon$ (6)

Load carrying capacity (7):

$$S = \sigma\{(1-1/\epsilon)^{1/2}\log[1 + 2\epsilon + 2\epsilon^{1/2}(1+\epsilon)^{1/2}] - 1\} \tag{7}$$

Zone width at $x = c$ and onset of cracking: $d = 0{\cdot}004$ in

Effective zone strain gradient at $x = c$ and onset of cracking: $\left(\frac{d\epsilon}{dx}\right)_e = 20\text{ in}^{-1}$

Fracture properties

Critical crack-tip strain and displacements:

a. Crack extension and stable growth: $\epsilon_c^* = 0{\cdot}24,\ v_c^* = 2{\cdot}6 \times 10^{-4}$ in

b. Crack propagation, $u > 10$ ft per sec: $\epsilon_c^* = 1{\cdot}1,\ v_c^* = 7 \times 10^{-4}$ in

Fracture toughness (f)

a. Onset of crack extension $K_c = 34$ ksi $\sqrt{\text{in}}$

b. Onset of unstable crack propagation $K_c = 37$ ksi $\sqrt{\text{in}}$

a. Obtained from tensile tests of strips

b. Obtained from compilation of data in Reference 5 and Fig. 1

c. This is an estimate based on the work of Embury, Keh, and Fisher [6]

d. Obtained from a correlation of ϵ and v measurements

e. An estimate based on metallographic sections of broken foils

f. Estimated from: $K_c = T^*\lambda\sqrt{(\pi c_0)}$, *where* c_0 is the initial slit length and λ is an elastic finite plate correction. The data involve c_0-values, in the range 0·110 in to 0·440 in and relatively low nominal stress values, $T^*/Y < 0{\cdot}6$

problem areas which appear to be involved in constructing an adequate quasi-static crack propagation model employing the Dugdale model. These arise in (a) specifying the flow stress-strain rate behavior of the material at high rates of strain, (b) evaluating the constraints imposed by necking, and (c) accounting for the finite dimensions of the specimen and its interaction with the testing apparatus. Although progress has been made in each individual area, a model in which all three elements are present has not been developed.

Strain-rate dependence of the yield stress

A previous compilation of the high strain rate data in the literature suggested a linear relation between Y and $\dot{\epsilon}$ at strain rates above 10^3 sec^{-1} [5]. The data could be fitted reasonably well by a line whose slope, F in Equation 3 of Table 1, was on the order of 25 psi-sec. In the intervening two years, the situation has become less certain. Five additional studies have appeared and these not only increase the scatter but cast doubt on the linearity of the relation (Fig. 1). Values of F of 10 and 25 psi-sec, which are used in the calculations reported below, bracket only about half the data. Until the situation can be resolved, accurate predictions of ductile crack speeds based on inputs from dynamic yield experiments are precluded.

Necking correction

A relation between the flow stress σ at each point in the plastic zone and the load carrying capacity S of that portion of the zone is required. A more realistic relation than that used previously [4] can be obtained from Bridgeman's [7] solution for the necking of a thin plate under tension. In this result the parameter a/R, the ratio of the half thickness of the neck to the radius of curvature of the outside surface of the neck, appears as an independent variable. Following Bridgeman's work on tensile bars, an empirical relation between a/R and the true strain at the neck was constructed, Equation 6, Table 1. Incorporating this information into Bridgeman's formula gives Equation 7, Table 1, which replaces Equation 10 of the previous calculation [4]. Otherwise, the basic equations of the superposition method and the computational scheme used earlier are essentially unchanged. Full details are given in Reference 4 and will not be repeated here.

Finite specimen size

To account for finite specimen dimensions, Hulbert, *et al.* [14] solved the static elastic boundary value problem in which a Dugdale crack is centrally located in a thin rectangular sheet. With their technique, called the boundary point least squares method, a series of stress functions, each containing an arbitrary constant, is selected. In particular, the complex variable

functions of the Kolsov-Muskhelishvili type automatically satisfying the symmetry conditions of the problem were chosen. As in the simple Dugdale model, plastic deformation is characterized by a uniform flow stress. The constants in the series were evaluated by satisfying the boundary conditions in the least squares sense at a large but discrete number of boundary points.

Among other conclusions, the finite plate studies have shown that v_c is closely approximated by Equation 2 even when the crack length is comparable to the plate width. On the other hand, the applied load necessary to obtain a given value of l or, equivalently, of v_c is well approximated by Equation 1 only when c and l are small relative to the plate width. Consequently, finite plate effects can be safely ignored in analyzing the extension of small slits but must be included in the treatment of the larger cracks encountered in the unstable propagation studies. The inertia of the specimen and the testing machine also influence the load acting on the specimen during the crack extension process. For the present, however, it is assumed consistent with experiment that the crack moves slowly in comparison to the wave speeds associated with the testing device and both the specimen and the machine are in static equilibrium throughout.

Two empirical relations for a Dugdale crack in a sheet having finite dimensions can be abstracted from the results generated with the boundary point least squares computer program [14]. The first is

$$b(c,\ T) = \pi \frac{Tc}{E} \csc \frac{\pi c}{h} \tag{8}$$

where b denotes the displacement of the clamped edge of the foil with respect to the crack line in the direction normal to the crack, $2h$ is the height of the foil, and T is the average applied stress. The second relation connects T and T_∞, the applied stress in an infinite plate which produces the same displacement for the same crack length:

$$\frac{T_\infty}{T} = \left\{ \sec \frac{\pi c}{2w} \right\}^{1/2} \tag{9}$$

where $2w$ is the width of the foil†.

The applied stress T acting at any stage of the crack extension process can be evaluated using these empirical relations. If the testing apparatus

† It should be emphasized that Equations 8 and 9 are based solely on the computational results of 3-½ × 4″ foils with uniform displacement boundary conditions and are, therefore, strictly applicable only to these conditions (which most nearly simulate the conditions under which the foil specimens were tested). The possibility of extending these relations to other geometries and boundary conditions has not been examined.

is completely elastic the additional displacement of the edge of the foil from that at the onset of crack extension will be directly proportional to the decrease in the force exerted by the apparatus. This can be expressed as

$$T = T_0 - k[b(c, T) - b(c_0, T_0)] \tag{10}$$

where T_0 is the applied stress acting to initiate crack extension at the initial crack length $2c_0$ and k is an elastic spring constant. Substituting Equation 8 into Equation 10 then gives for the variation of the load as a function of the crack length

$$\frac{T}{T_0} = \frac{\frac{\pi k c_0}{E} \csc \frac{\pi c_0}{h} + 1}{\frac{\pi k c}{E} \csc \frac{\pi c}{h} + 1} \tag{11}$$

A simplified expression for crack speed is derived in Reference 4 for the special case of a uniform flow stress with a linear rate dependence. This can be written

$$U = \frac{Y_S}{F\left(\frac{\Delta\epsilon}{\Delta x}\right)_c}\left[\frac{Y}{Y_S} - 1\right] \tag{12}$$

where Y_S, F, and $(\Delta\epsilon/\Delta x)_c$ are regarded as material constants. Now, by combining Equations 1 and 2 and using Equation 9, a transcendental equation for Y can be obtained. Introducing the experimental observation that the crack will propagate with a constant crack-tip displacement [4], this relation can be solved to give $Y = Y(c, T)$. Thus, by making use of Equations 11 and 12, crack speeds can be calculated as a function of crack length. In particular, for the two extreme cases which can be identified, $k = 0$ (dead loading) and $k = \infty$ (fixed grips).

Experimental techniques

Experiments were performed on a heavily cold rolled 0·00175 in-thick†, plain carbon steel foil [4], whose mechanical properties are listed in Table 1.

Measurements of the plastic zone, both before crack extension and during stable growth, were performed on foil coupons with a gage section

† The original thickness of the foil was 0·00185 in and this was reduced to 0·00175 in in the course of electropolishing the surface to enhance the reflectivity. Thickness values were obtained from metallographic sections with a calibrated microscope to a precision of about ± 0·00005 in. These showed that the foil is quite uniform with the thickness varying no more than about ±5%.

3·9 in-wide by 4 in-long. Centrally located slits 0·006 in-wide of length $2c = 0·220$ in, 0·440 in, and 0·880 in, were introduced by spark machining normal to the rolling direction. Deformation produced by these slits under load was predominantly through-the-thickness and concentrated in a small segment of the slit root radius (see Figs. 2 (a) and 2 (b)) which suggests that the slits behaved more like sharp cracks than the root radius would imply.

The coupons were cemented into grips and loaded in a small tensioning device which could be mounted on a standard interferometric microscope. In this way, it was possible to photograph the interferometric pattern produced by the yielded (necked) region near the tip of the slit at predetermined stress levels while the foil was *under load* (see example in Fig. 2 (a)). Observations at high magnification also pinpointed the onset of crack extension and the amount of stable crack growth.

Crack speed measurements were derived from high speed motion picture records (3300 frames per sec) of 3·25 in by 3·5 in foil coupons with slits of length $2c = 0·220$ in broken under dead load in a creep machine. The crack-tip strain and displacement cited for the propagating cracks in Table 1 were derived from highly magnified metallographic sections of the broken foil. Details of these experiments are contained in Reference 4.

Results

Local yielding

The interferometric pattern of the plastic zone ϵ_z, the through-the-thickness strain distribution, which can be presented graphically in several ways [3, 15]: (a) by isostrain contours, Fig. 2 (b), (b) by ϵ_z-profiles on sections along the plastic zone, Fig. 2 (c), and (c) by the gradient of ϵ where ϵ is the largest value of ϵ_z on any section, Fig. 3 (a). These results illustrate that the foil embodies many of the idealizations of the Dugdale model such as elongated, wedge-shaped zones. This shape and the fact that the zones are necked largely preclude in-plane strain and lead to the approximation $\epsilon_y = -\epsilon_z$. A further consequence is that v, the y-direction displacement produced by plastic deformation within the zone, can be deduced from the area inscribed by the ϵ_z-profile in Fig. 2 (c)†.

Values of ϵ of each point of the zone are approximated by a single valued function of v independent of position or stress level (Equation 5, Table 1). This implies that each element of the foil in the path of the growing crack experiences the same stress-strain history, an assumption implicit in the analysis. Finally, Fig. 3 (a) shows that the strain distribution measured in the foil near the slit is closely matched by the distribution obtained

† $2v = -\int_{-\infty}^{\infty} \epsilon_z dy$

analytically.† Deviations at large distances indicate that the model overestimates the measured zone length possibly because model zones are, proportionately, even narrower than those of the foil.

Onset of crack extension

Fig. 3 (a) illustrates that the strain distributions measured at the same *K*-level‡ are indistinguishable even though substantially different slit lengths and stress levels are involved, and the strain distributions coinciding with the onset of stable crack extension are also indistinguishable. It follows that crack extension in the foils will obey a stress intensity criterion at low nominal stress levels, e.g., when $T^* < 60$ ksi ($T^*/Y < 0{\cdot}6$) in Fig. 4 (c).

The invariance of the strain distribution existing at the onset of crack extension appears to be related to ϵ_c, the crack-tip strain and v_c, the crack tip displacement.§ As shown in Figs. 3 (a) and 4 (b), crack extension begins when $\epsilon_c = 0{\cdot}24 \pm 0{\cdot}03$ independent of slit length or stress level, and this is regarded as a critical value, $\epsilon_c{}^*$. The same value of $\epsilon_c{}^*$ is maintained throughout the stable growth period until the onset of unstable propagation (see Figs. 3 (b) and 4 (b)).

Furthermore, the existence of a constant, limiting $\epsilon_c{}^*$ is consistent with:

(a) McClintock's [16-18] analysis of the micromechanics of ductile rupture taken together with the invariance of stress-strain history within the zone

(b) The fact that rupture is confined to the immediate vicinity of the slit or crack tip, and

(c) The existence of a limiting crack-tip displacement (see Fig. 3 (a)) as postulated by Wells [19], since ϵ and v are related.

Values of T^* and K_c, the nominal stress and stress intensity coinciding with the onset of crack extension were derived using the super-position method together with Equations 4-7 and by the limiting value of the crack-tip strain [3]. As shown in Figs. 4 (c) and 4 (d), the calculated values are in accord with the measurements, a result which is not surprising since the strains close to the slit are accurately described by the model.

Stable crack growth

The onset of crack extension at $K_c \approx 34$ ksi $\sqrt{\text{in}}$ is followed by a short interval where the crack grows with increasing stress but does not become

†Calculated from the basic displacement relation and the flow properties of the foil as described by Equations 4-7.

‡$K \equiv T\lambda\sqrt{\pi c}$ is the stress intensity, where T is the net section stress, 2c the slit length and λ an elastic finite specimen-size correction.

§The interferometric patterns are actually very difficult to interpret right at the tip of the slit or growing crack. Values of ϵ_c and $\epsilon_c{}^*$ were therefore always measured 0·001 in from the slit or crack tip.

unstable. A second toughness value, $K_c \approx 37$ ksi $\sqrt{\text{in}}$† marks the transition from slow growth to fast fracture, and this can be regarded as the 'ultimate' strength of a cracked coupon. Observations of stable growth in the foil are especially interesting because the growth is neither accompanied by nor complicated by change in the fracture mode. The amounts of stable growth observed, $\Delta c/c_0 = 0{\cdot}05$-$0{\cdot}28$, are in the same range as the values reported by McClintock [16] for aluminum foil. Fig. 3 (b) shows that the zones are visibly longer after slow growth, but the strain distribution near the crack tip is unchanged. The zones observed just before the onset of fast fracture are consequently more closely approximated by the calculated gradient in Fig. 3 (a) than the pre-growth zones. Since the Dugdale model has no provisions for stable growth, the agreement is fortuitous. However, the fact that the model does reproduce the gradient existing at the onset of fast fracture lends support to the crack propagation calculations.

Unstable crack propagation

Sections of the foil ruptured by unstable cracks propagating at speeds from about 10-300 ft per sec show roughly constant values of $\epsilon_c{}^* \approx 1{\cdot}1$ and $v_c{}^* \approx 7 \times 10^{-4}$ in‡ [9]. This invariance simplifies the task of calculating crack speed by the two methods that have been discussed. The results of such calculations, showing the relative contributions of the rate sensitivity coefficient, the necking correction, and finite plate effects, are presented in Fig. 5. It is apparent that each of these three factors exerts a strong influence on the calculated values. The comparisons with experiments are also intended to illustrate that the analysis can be fitted to the measurements with reasonable values of the coefficients. For example, the comparison in Fig. 5 is only meaningful as long as the coupon can be approximated by an infinite plate, i.e., as long as the c/w ratio is small. Fig. 5 illustrates that the correspondence extends to large values of c/w when the finite dimensions of the coupon and end conditions are taken into account.

The results demonstrate a measure of internal self consistency: the value $F = 10$ psi-sec together with a necking correction (Fig. 5 (a)) appears to be roughly equivalent to $F = 25$ psi-sec without a necking correction (Fig. 5 (b)). However, too much significance cannot be attached to the agreements seen in Fig. 5. For one thing, the rate sensitivity is not well known; even the range 10 psi-sec $< F <$ 25 psi-sec does not bracket all the high rate flow measurements reported for steel. Secondly, while agreement with a dead load solution is plausible, this too involves uncertainties, since the dynamic response of the creep machine was not determined.

†This value is based on the initial slit length.

‡While these values are substantially larger than those observed during stable growth, they are consistent with the ϵ-v relation used earlier.

Discussion

The cold rolled steel foil comes close to reproducing in the laboratory two idealizations: (a) the elastic-perfectly plastic material and (b) crack extension under plane stress. The Dugdale-like zones are unquestionably a result of the lack of strain hardening coupled with the ease of through-the-thickness strain. The same foil displays even narrower zones in an annealed condition [14] with a sharp yield drop that is equivalent to a negative strain hardening rate. However, when the foil is notched after it has been both annealed and prestrained into the range where it strain hardens significantly, it displays broader zones more like those calculated by Swedlow, *et al.* [20]. The results for the foil thus illustrate some general principles and are especially relevant for thin, heavily worked or low strain hardening materials.

The lack of hardening causes necking as soon as yielding begins and this contributes to the strain concentration generated at the crack tip. However, the necked regions derive support from the surrounding material and do not become unstable even though the macroscopic necking strain, essentially zero for the foil, is exceeded. This is entirely consistent with a simplified analysis of necking instability within a Dugdale zone given in an earlier paper [15], which shows that the instability condition is a function of the stress-strain distribution along the entire zone and not just the necking strain. While these results cast doubt on Krafft's ligament instability criterion [21] which identifies $\epsilon_c{}^*$ with the macroscopic necking strain, they do not negate the importance of strain hardening in mitigating strain concentrations or the concept of a critical strain. However, the critical strain should be regarded as a fracture property of the material which is governed by the microscopic ductile rupture process and is sensitive to the stress-states and strain rates generated near the crack tip. A simple mathematical expression of these ideas derived previously [3, 15, 22]:

$$K_c \approx \sqrt{0{\cdot}5EY\epsilon_c{}^* d} \tag{13}$$

gives $K_c = 39$ ksi $\sqrt{\text{in}}$† which is very close to $K_c = 34$ ksi $\sqrt{\text{in}}$, the value actually measured for the foil. Similarly for 0·082 in-thick maraging steel aged to peak hardness [23], a condition which also displays little strain hardening, the prediction ‡$K_c = 222$ ksi $\sqrt{\text{in}}$ is very close to the measured value $K_c = 218$ ksi $\sqrt{\text{in}}$.

The Dugdale crack does not lend itself to the treatment of stable crack growth because it is difficult to model the residual stresses that develop within the plastic region left behind by the growing crack. A treatment of

† For the steel foil $E = 30{,}000$ ksi, $Y = 105$ ksi, $\epsilon_c = 0{\cdot}24$, d (the width of the zone near the crack tip at failure) = 0·004 in.
‡ For maraging steel $E = 30{,}000$ ksi, $Y = 269$ ksi, $\epsilon_c = 0{\cdot}10$, $d = 0{\cdot}123$ in.

stable growth under antiplane strain has been derived by McClintock [16-18] and this suggests how flow and fracture affect stable growth. However, there is some question whether the analysis is generally and directly applicable to simple tension.†

The Dugdale crack offers insights into ductile crack propagation. The calculations presented in this paper tend to support the idea that the speed of ductile fracture is limited by the rate of plastic flow ahead of the crack. The analysis identifies the important contributions to the propagation process: (a) the absolute value of the yield stress, (b) $\epsilon_c{}^*$, (c) the ϵ-v relation and ϵ-gradient which are influenced by the strain hardening rate, (d) the rate sensitivity of flow, (e) necking, (f) finite plate dimensions and end conditions, and (g) the dynamic response of the testing machine. Further testing of the analysis is hampered by the dearth of reliable high-strain-rate flow stress data. Ultimately, however, it may be possible to reverse the procedure and extract high-strain-rate flow data from crack-speed measurements.

Acknowledgments

The authors are grateful to the Army Research Office, Durham, for sponsorship of the research. Expert assistance was provided by Mr. C. R. Barnes with the experiments and Miss C. Pepper with preparation of the manuscript. The foil was kindly supplied by Dr. E. T. Stephenson of the Bethlehem Steel Corporation. Several useful contributions were made by Dr. A. K. Mukherjee during the early phases of this study.

References

1. DUGDALE, D. S. 'Yielding of steel sheets containing slits'. *J. Mech. Phys. Solids*, vol. 8, p. 100. 1960.
2. GOODIER, J. N. and FIELD, F. A. 'Plastic energy dissipation in crack propagation' Drucker and Gilman, eds. *Fracture of Solids*, Interscience, New York, 1963, p. 103.
3. ROSENFIELD, A. R., DAI, P. K., and HAHN, G. T. 'Crack extension and propagation under plane stress', *Proceedings of the First International Conference on Fracture, Sendai, Japan*, 1965, p. 223.
4. KANNINEN, M. F., MUKHERJEE, A. K., ROSENFIELD, A. R., and HAHN, G. T. 'The speed of ductile-crack propagation and the dynamics of flow in metals', *Symposium on the Mechanical Behavior of Materials under Dynamic Loads*, Springer-Verlag, New York, in press.
5. ROSENFIELD, A. R. and HAHN, G. T. 'Numerical descriptions of the ambient low-temperature, and high-strain rate flow and fracture behavior of plain carbon steel'. *Trans ASM*, vol. 59, p. 962. 1966.

† The McClintock analysis suggests that long cracks display proportionately less stable growth than short ones, and while this is in accord with his own experiments, it is contrary to both the experience with the steel foil (see Fig. 2 (b)) and to Broek's [24] results for aluminum alloys.

6. EMBURY, J. D., KEH, A. S., and FISHER, R. M. 'Substructural strengthening in materials subject to large plastic strains'. *Trans Met. Soc. AIME*, vol. 236, p. 1252, 1966.
7. BRIDGEMAN, P. W. *Studies in large plastic flow and fracture*, Harvard University Press, Cambridge, Mass., 1964, p. 36.
8. KANNINEN, M. F. 'An estimate of the limiting speed of a propagating ductile crack'. *J. Mech. Phys. Solids*, in press.
9. HARDING, J. 'The effect of grain size and strain rate on the lower yield stress of pure iron at 288°K. Report No. 1,037.67, Department of Engineering Science, University of Oxford, 1967.
10. DOWLING, A. R. and HARDING, J. 'A comparison of strain rate effects in mild steel under tensile and punch loading', *Proceedings of the First International Conference of the Center for High Energy Forming*, Estes Park, Colo., in press.
11. OXLEY, P. L. B. and STEVENSON, M. G. 'Measuring stress/strain properties at very high strain rates using a machining test'. *J. Inst. Met.*, vol. 95, p. 308. 1967.
12. WILSHAW, T. R. and KELLY, J. M. *Response of circular clamped plates to square wave stress pulses*. Report SU-DMS No. 67-36, Department of Materials Science, Stanford University, Stanford, California, 1967.
13. BUTCHER, B. M. and MUNSON, D. E. 'The application of dislocation dynamics to impact-induced deformation under uniaxial strain', Rosenfield, Hahn, Bement. and Jaffee, eds. *Dislocation Dynamics*, McGraw-Hill, New York, 1968, p. 591.
14. HULBERT, L. E., HAHN, G. T., ROSENFIELD, A. R. and KANNINEN, M. F. 'An elastic-plastic analysis of a crack in a plate of finite size', *Proceedings of the 12th International Congress of Applied Mechanics*, Stanford, California, in press.
15. HAHN, G. T. and ROSENFIELD, A. R. 'Local yielding and extension of a crack under plane stress'. *Acta Met.*, vol. 13, p. 293. 1965.
16. McCLINTOCK, F. A. 'Ductile fracture instability in shear'. *J. Appl. Mech.*, vol. 25, p. 582. 1958.
17. McCLINTOCK, F. A. 'On the plasticity of the growth of fatigue cracks', Drucker and Gilman, eds. *Fracture of Solids*, Interscience, New York, 1963, p. 65.
18. McCLINTOCK, F. A. and IRWIN, G. R. 'Plasticity aspects of fracture mechanics', ASTM STP No. 381, *Fracture Toughness Testing and its Applications*, 1965, p. 84.
19. WELLS, A. A. 'Application of fracture mechanics at and beyond general yielding'. *Brit. Weld. J.*, vol. 10, p. 855, 1963.
20. SWEDLOW, J. L., WILLIAMS, M. L. and YANG, W. H. 'Elastoplastic stresses and strains in cracked plates', *Proceedings of the First International Conference on Fracture, Sendai, Japan*, 1965, p. 259.
21. KRAFFT, J. M. 'Correlation of plane strain crack toughness with strain hardening characteristics of a low, a medium, and a high-strength steel'. *Appl. Matls. Res.*, vol. 3, p. 88. 1964.
22. HAHN, G. T. and ROSENFIELD, A. R. 'Sources of fracture toughness: the relation between K_{I_c} and the ordinary tensile properties of metals'. ASTM STP No. 432, *Applications Related Phenomena in Titanium Alloy*, 1968, p. 5.
23. HAHN, G. T., MUKHERJEE, A. K., and ROSENFIELD, A. R. 'Plastic zone formation and stable crack growth in high-strength alloy sheets', *Engg. Fracture Mech.*, in press.
24. BROEK, D. *The residual strength of cracked sheet-tests interrupted after intermediate slow crack growth*. Report No. NLR-TR M. 2145, National Aerospace Laboratory, Amsterdam, 1965.

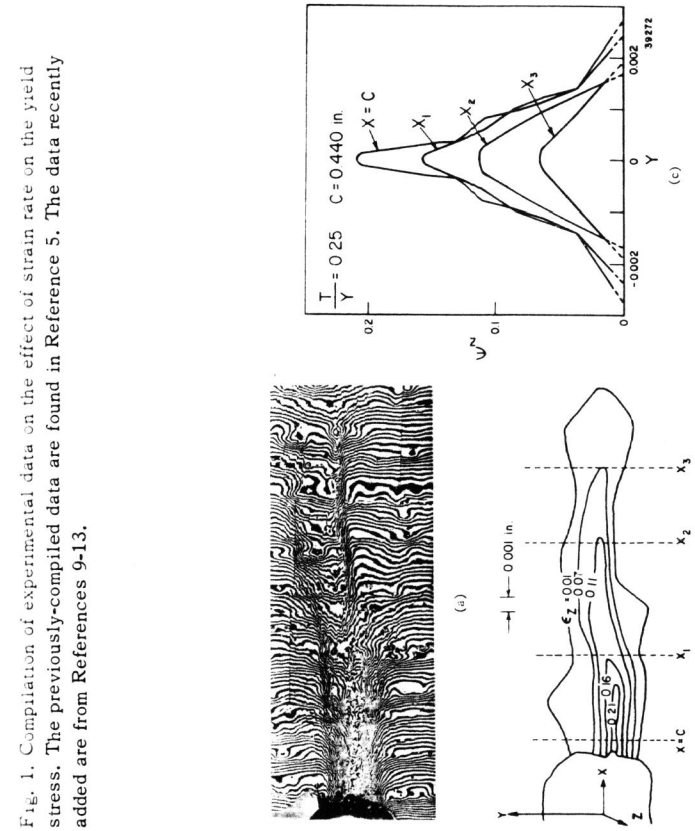

Fig. 2. Strain distribution ahead of a slit revealed under load by interferometric fringe pattern: (a) fringe pattern displayed by sample with $c = 0{\cdot}440$ in loaded to $T/Y = 0{\cdot}25$, $K/Y = 0{\cdot}30\sqrt{\text{in}}$, (b) the isostrain contours derived from the fringes, and (c) the ϵ_z-strain profile at four points along the plastic zone. (a) and (b) 150×

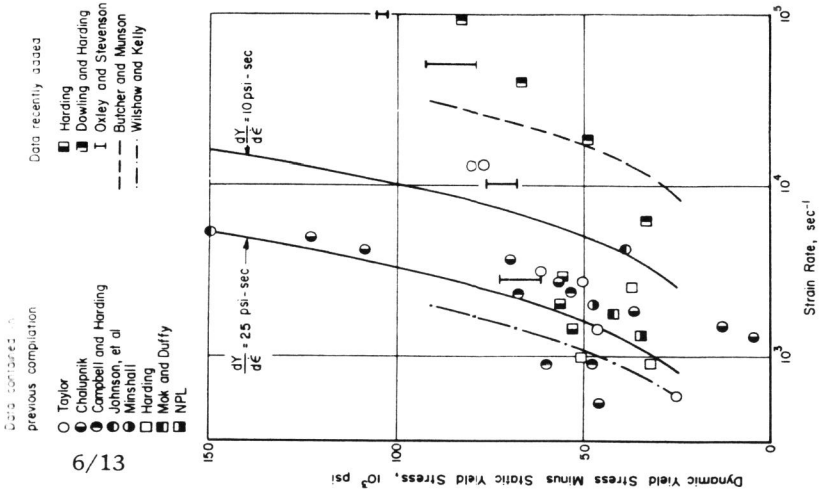

Fig. 1. Compilation of experimental data on the effect of strain rate on the yield stress. The previously-compiled data are found in Reference 5. The data recently added are from References 9-13.

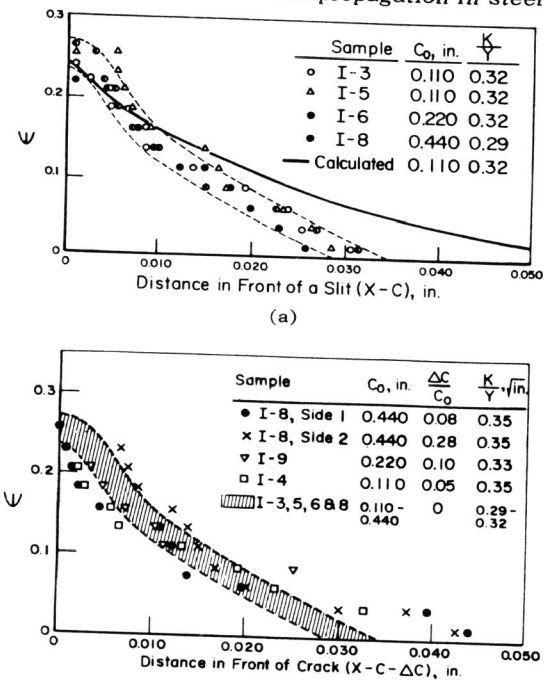

Fig. 3. Comparison of measured strain gradients with the gradient calculated from the Dugdale model: (a) gradients existing just before the onset of stable crack growth and (b) gradients observed during the stable growth stage.

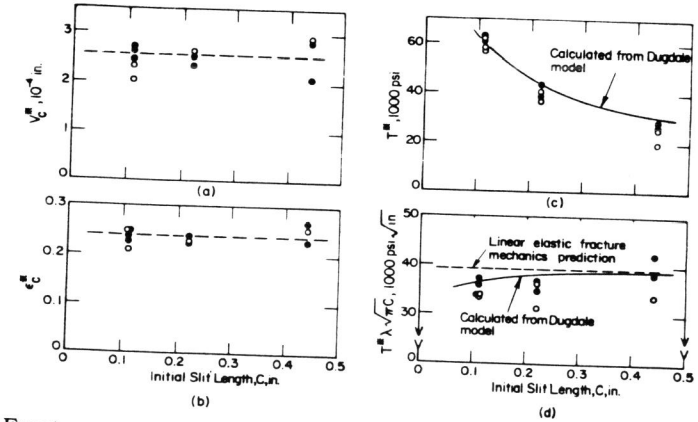

Fig. 4. Fracture parameters: (a) crack-tip displacement at the onset of cracking, (b) peak crack-tip strain at the onset of cracking, (c) nominal (net section) stress at the onset of cracking, and (d) fracture toughness parameter. Open data points show the value at the onset of crack extension; solid points, the value just prior to unstable fracture.

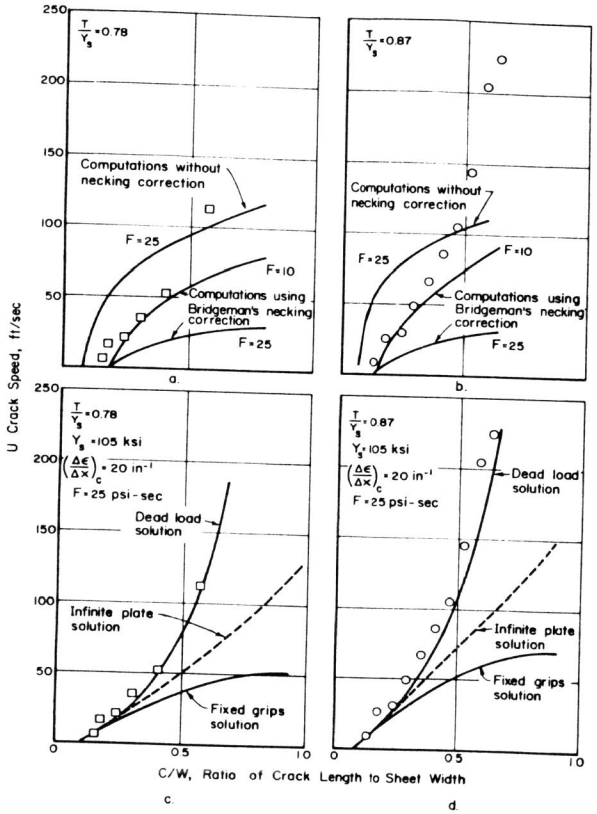

Fig. 5. Comparison of calculated and observed crack speeds in steel foil: (a) and (b) superposition method applied to an infinite plate, and (c) and (d) uniform flow stress-finite plate method.